Analysis of a High Velocity Oxygen-Fuel (HVOF) Thermal Spray Torch, Part 2: Computational Results*

DRAFT

William L. Oberkampf
Aerodynamics Dept., Org. 1554
Sandia National Laboratories
Albuquerque, NM 87185-0825

Milind Talpallikar
CFD Research Corporation
3325 Triana Blvd.
Hunstville, AL 35805

Abstract

The fluid dynamics inside and outside a High Velocity Oxygen-Fuel (HVOF) torch are analyzed using computational fluid dynamic (CFD) techniques. The thermal spray device analyzed is similar to a Metco Diamond Jet torch with powder injection. The spray nozzle is axisymmetric with powder injected on the centerline, premixed fuel and oxygen fed from an annulus, and air cooling injected along the interior surface of the aircap. Choked flow conditions occur at the exit of the aircap and a supersonic, under-expanded jet develops externally. The details of the CFD simulation are given in a companion paper [3]. This paper describes the general gas dynamic features of HVOF spraying and then gives a detailed discussion of the computational predictions of the present analysis. The gas velocity, temperature, pressure and Mach number distributions are presented for various locations inside and outside the torch. Characteristics of the metal spray particle velocity, temperature, Mach number, trajectory, and phase state (solid or liquid) are also presented and discussed. Extensive numerical flow visualization is provided to show flow features such as mixing layers, shock waves, and expansion waves.

THERMAL SPRAYING using the High-Velocity Oxygen-Fuel (HVOF) process is being used in an increasing variety of coating applications. Metallic, ceramic and composite coatings are being applied to substrates to improve wear-resistance, abrasion resistance, thermal and electrical insulation, and corrosion protection. Coatings applied using HVOF spraying have proven to be of high density, good bond and mechanical strength, and a thermal expansion coefficient near the substrate material. HVOF spray torches use a combustion process to heat the gas flow and the coating material and then accelerate the gas/particle two-phase flow to high velocities. The gas and particle velocities are commonly much higher than those achieved using plasma spraying.

The sophistication of numerical simulations for thermal spraying has greatly improved during the last few years. This improvement in modeling the complex physics in thermal spraying has been brought about by both improved numerical modeling and the application of computational

* Part of this work was performed at Sandia National Laboratories, which is operated by Martin-Marietta Corp. for the U. S. Department of Energy under contract No. DE-AC04-94AL85000.

techniques developed for liquid and solid rocket motors. Axisymmetric and planar two-dimensional computational fluid dynamic (CFD) simulations of chemically reacting, dissociated and ionized flow, two-phase flows, along with state of the art turbulence models, has been presented in the literature. Power, Barber, and Chiappetta [1] and Smith, et al. [2] conducted the first CFD simulation of the HVOF spraying process. They modeled the internal and external flow of the Metco Diamond Jet torch. In this torch, powder is fed through a center tube using nitrogen as a carrier gas. Premixed oxygen and propylene are injected through an annulus in the nozzle. This annulus is a simplification of the eight small holes in the nozzle to introduce pre-mixed fuel and oxygen. Air is injected in an outer annulus in the nozzle for the purpose of cooling the aircap, as the torch has no other cooling mechanism. The combusting flow was modeled inside the converging aircap and the flow became choked at the exit of the aircap, that is, attained the sonic condition. External to the torch, they modeled the decay of the supersonic jet in a quiescent atmosphere. As the pressure in the torch was greater than atmospheric at the exit, the jet was under-expanded. The flow then expanded exterior to the aircap and formed "shock diamonds" commonly seen in supersonic, under-expanded streams. Their CFD simulation included a k-ε turbulence model and combustion chemistry. Their chemistry model included dissociation of the reaction products using an approximate equilibrium model and seven gas species; C_3H_6, O_2, N_2, H_2O, CO_2, CO, and H_2. Because of uncertainties in their combustion model, they modeled the internal and external flow separately, that is, the converged solution for the internal flow was used as the specified inflow for the external flow solution. They assumed fully mixed, i. e., uniform, flow out of the aircap as the supersonic inflow conditions for the exterior flow solutions. The finite difference equations, using a density based formulation, were solved by an explicit time iterative scheme. Particles of various sizes were injected inside the aircap near the centerline but these particles did not interact in any way with the gas stream. They were tracker particles responding to the local gas velocity and temperature but did not change the flow. Their analysis also did not account for any phase change of the particles.

This paper describes the general gas dynamic features of HVOF spraying and then gives a detailed discussion of the numerical predictions of a computational fluid dynamic (CFD) analysis. A companion paper [3] presents the detailed formulation and numerical methods of the CFD analysis. The HVOF torch analyzed is similar to the Metco Diamond Jet torch. The gas velocity, temperature, pressure and Mach number distributions are presented for various locations inside and outside the torch. Characteristics of the metal spray particle velocity, temperature, Mach number, trajectory, and phase state (solid or liquid) are also presented and discussed. Extensive numerical flow visualization is provided to show flow features such as mixing layers, shock waves, and expansion waves.

General Flow Field Characteristics

Internal Flow. Various types of HVOF thermal spray torches have different internal

methods for introducing the material to be sprayed and the fuel and oxygen. Each design produces distinct gas dynamic, combustion, heat transfer, and particle dynamics characteristics. The geometry chosen for the present analysis is similar to the Metco Diamond Jet torch, but there are notable differences. Figure 1 shows the detailed internal geometry of the conceptual torch analyzed. Although this geometry does not match precisely any existing torch design, it does represent an HVOF geometry that captures all of the important gas dynamic and two-phase flow features typical of HVOF spray torches. The conceptual torch is assumed to be a two-dimensional axisymmetric geometry. The central stream uses argon as the carrier gas to inject solid particles through a circular tube. The present analysis assumed spherical particles of a well characterized, low melting temperature material, copper. The second stream injects premixed propylene and oxygen through an annulus at an angle of 5^{o} to the centerline. In the Metco Diamond Jet torch, premixed propylene and oxygen are injected through eight small tubes circumferentially spaced equally around the nozzle. In order to keep the analysis tractable, a two-dimensional axisymmetric annulus for injection of fuel and oxygen is assumed. In the actual Diamond Jet torch, however, the flow around each fuel/oxygen injection port is a three-dimensional flow field. The third stream injects air through an annulus also at an angle of 5^{o} adjacent to the wall for cooling of the aircap. The aircap geometry is a 5^{o} half-angle, conically converging nozzle that attains a minimum area at a distance of 10 mm from the injection location. The torch is assumed to exhaust to ambient conditions consisting of air at room temperature and pressure.

The central stream of argon and particles is typically injected at room temperature and at low velocity, Mach number less than 0.1. The oxy-propylene and air streams are typically higher speed streams with a Mach number in the range 0.3 to 0.6, depending on the mass flow settings for the gases. The Mach number of the incoming streams also depends on the operating pressure inside the aircap. As the incoming streams are subsonic, the pressure at the exit of the nozzle channels must match the pressure inside the aircap. Therefore, the density of the incoming gases changes which, in turn, affects the inflow Mach number. For example, when the aircap is removed and the torch is ignited, the oxy-propylene jets become supersonic because the ambient pressure is reduced compared to the aircap operating pressure.

The release of thermal energy from the oxy-propylene combustion causes a sufficient increase of pressure inside the aircap so that the aircap chokes at the exit. If the torch is not ignited, i. e., combustion does not occur, the total mass flow rate of the various gas streams is not sufficient to choke the flow at the exit of the aircap. Once the torch is ignited, the torch remains lit because of the separated flow regions formed at the face of the nozzle. These separated, or reversed, flow regions serve as a flame holder for hot combusting gases to ignite the incoming fuel/oxygen stream. The character of these separated flow regions is very similar to the flow in the base region of rocket powered missiles. If these separated flow regions are eliminated, the torch will not stay lit because the flame speed is much less than the incoming fuel/oxygen gas speed. The reaction zone, or flame front, spreads across the premixed oxy-propylene stream as it mixes with the air and argon/particle streams. Note that this ignition character of the premixed oxy-fuel stream

is not in the present reacting flow model. As discussed in Ref. 3, the present model assumes an approximate equilibrium chemistry model. This results in an infinite reaction rate, essentially a detonation, of the fully mixed streams as soon as they enter the computational domain.

Near the face of the nozzle, four free-shear layers exist between the mixing streams; one between the argon/particle stream and the adjacent nozzle base flow, two between the oxy-propylene stream and the nozzle base flow (one on each side of the oxy-propylene stream), and one between the air stream and the nozzle base flow. In addition, the air stream continues forming a boundary layer, i. e., an attached shear layer with the aircap wall. Under normal operating conditions, each of these shear layers is turbulent along with the incoming streams.

External Flow. The pressure in the aircap is sufficient to choke the flow through the nozzle exit, that is, Mach one is attained at the exit of the aircap. As the pressure in the exit plane is typically greater than the ambient condition, the aircap flow is said to be under-expanded. The flow will expand supersonically external to the nozzle so as to meet the ambient pressure condition. The external pressure adjustment of the supersonic stream occurs through an alternating series of expansion and compression waves. Figure 2 shows a simplified sketch of the expansion, compression, and shock waves in the supersonic jet along with the free-shear, or mixing, layer surrounding the jet. The angle of the expansion and compression waves with respect to the local gas velocity is well known from fundamental gas dynamics to be $\sin^{-1}(1/M_l)$, where M_l is the local Mach number.[1] If it is assumed that the flow is uniform in the exit plane and the Mach number is unity, the angle of the first wave emanating from the edge of the exit is at an angle of 90^o. The angle of the last wave is determined by the Mach number to which the flow must expand in order to decrease the pressure to the ambient conditions. The pressure in the outer portion of the mixing layer is constant at a value equal to the ambient pressure. To simplify the wave pattern in Fig. 2, the waves are shown as straight lines, when in reality they are curved because the local Mach number varies across the stream.

The expansion waves intersect the mixing layer on the periphery of the jet and are reflected as compression waves. It is well known that waves in supersonic flow reverse character when they intersect a constant pressure boundary , i. e., a free-jet boundary. Figure 2 shows the waves penetrating the mixing layer up to the sonic line in the shear layer. The turbulent mixing layer represents the region of large velocity gradient where the flow changes from supersonic speeds to near zero velocity in the ambient flow. The compression waves coalesce into a normal shock wave near the centerline and into an oblique shock wave near the mixing layer. The flow after the shock waves raises the temperature of the gas substantially such that the gas luminesces. These high temperature embedded regions are normally referred to as "shock diamonds." The oblique shock wave intersects the free-shear layer and reflects as a "fan" of expansion waves. This expansion fan nearly duplicates the original expansion fan originating from the corner exit plane of the aircap. If viscosity did not exist, i. e., assuming inviscid flow, the series of expansion/compression/shock waves would repeat indefinitely. Because of viscosity, however, the mixing layers eventually met

[1]The local Mach number is the ratio of the local velocity to the local speed of sound. Mach number is not a dimensionless velocity, but a scaled velocity.

on the centerline after several shock diamonds. The length of the visible shock-diamond plume indicates the longitudinal extent of the supersonic flow. The supersonic flow eventually decays to subsonic conditions throughout the jet while entraining increasing amounts of cool ambient air. (See Hackett, Settles, and Miller [4] for an excellent description of the free-jet mixing process in HVOF torches.)

Discussion of Computational Results

Internal Flow Field. Figure 3 shows the computed temperature distribution inside the aircap using shaded contours. Recall that the premixed oxy-propylene stream enters from the nozzle between a radial position of 2.5 and 3 mm. This can be seen as the small region of cool gas (313 K) entering from the nozzle on the left. The chemistry model includes nine gas species; C_3H_6, O_2, CO_2, CO, H, H_2, H_2O, O, and OH. The model takes into account the dissociation of the gaseous combustion products. If dissociation of the gases is not included in the chemistry model, then the temperatures predicted will be unrealistically high, roughly by a factor of two for the present fuel and oxygen reactants. The peak combustion temperature for the present simulation is 3100 K and this occurs very near the oxy-fuel inlet. The chemistry model also assumes instantaneous reaction of the pre-mixed oxy-propylene stream as soon as it enters the computational domain. Physically this implies that the combustion energy, i. e., enthalpy, is released in the first line of computational cells near the oxy-propylene inlet. This results in a "detonation" of the pre-mixed fuel and oxygen in the computational domain. An improved chemistry model would use finite rate chemistry to model the gradual ignition of the oxy-fuel stream over a finite axial distance. Although this would provide an improved energy release model, computational time for a solution would increase substantially.

As can be seen from Fig. 3, the high temperatures persist in the core of the combusting oxy-propylene jet through most of the length of the aircap. At the exit plane the peak temperature is 2600 K. The combusting jet mixes moderately with the argon/particle stream, primarily because it is directed 5^o inward toward the centerline. Because of the low mixing, the temperature near the centerline at the exit of the aircap is only 600 K. Very little mixing of the combustion gases occurs with the air stream near the aircap wall. This computationally demonstrates the effectiveness of the air cooling technique for the aircap.

The Mach number contours inside the aircap are shown in Fig. 4. Recall that the local Mach number is the ratio of the local gas velocity to the local speed of sound and that the local speed of sound is proportional to the square root of the local static temperature. The rapid release of energy near the oxy-fuel inlet causes a factor of 10 increase in temperature, resulting in a factor of 10 decrease in density. This generates high velocities and supersonic flow near the inlet, as if the oxy-fuel stream entering were an under expanded supersonic jet. This supersonic jet goes through expansions, compression, and shock diamonds just as the under expanded supersonic jet discussed in the previous section. Although the supersonic jet characteristic is a result of the

equilibrium chemistry assumption, this would not occur in reality because of finite rate reactions. If all chemical reactions occur inside the aircap, however, the present equilibrium model should produce qualitatively correct Mach numbers and velocities inside the aircap.

Because of the three co-axial streams, with one reacting, the flow is extremely non-uniform at the exit of the aircap. One-third of the exit plane flow (near the centerline) is subsonic. The middle third of the flow annulus is supersonic with the peak Mach number of 1.4. The outer third annulus is a nearly uniform Mach one flow. This presents a much more complex stream for expansion than discussed in the previous section. There the Mach number of the under expanded jet was unity in the exit plane and the velocity and temperature were uniform.

Figure 5 shows the axial velocity component vs radial position for x = 3, 6, and 9 mm from the face of the nozzle. This plot clearly shows the development of the velocity profiles through each of the three co-axial streams, including the mixing layers between each stream. The thickness of the turbulent boundary layer on the aircap wall can be seen as the sharp decrease in velocity at the wall. The boundary layer thickness is roughly 0.15 mm. The peak velocity of the combustion gases remains nearly constant, away from the oxy-fuel inlet, at a value of 1500 m/sec. Mixing of the high velocity combustion gases with the argon/particle streams is more effective than with the air cooling layer because the oxy-fuel stream is directed inward and because the core flow is at a lower velocity. But because of the radius of the core flow, however, the velocity on the centerline at the exit of the aircap is only 200 m/sec.

Contours of the computed (static) pressure distribution inside the aircap are shown in Fig. 6. It is seen from this plot that the pressure in the aircap is essentially constant, except for large variations near the inlet of the oxy-propylene stream and near the exit of the aircap. As discussed earlier in the contours of Mach number, Fig. 4, the expansion and compression regions associated with the supersonic jet are also seen in the pressure contours. Away from the jet, however, the pressure over the majority of the aircap is at a constant value near 250 kPa absolute (2.5 atm). As the flow nears the exit plane the pressure begins to decrease as the flow accelerates. Correct prediction of pressure levels in the aircap is important to the validation of the CFD simulations. The correct pressure prediction indicates qualitatively the accuracy of the reacting flow model. As the flow in the aircap is choked primarily because of the energy release from combustion, correct prediction of pressure is an indication of the combustion modeling accuracy. The CFD analysis of Power, et al. [1,2] on a similar torch geometry and gas flow rates yielded a pressure of 3 atm. In preliminary comparison with experimental pressure measurements, they found predicted pressures higher than experiment. Future related work on HVOF spraying will measure the pressure at different locations inside the aircap and for various operating conditions. These measurements will then be compared to CFD predictions matching the torch geometry and flow rates.

External Flow Field. Figure 7 shows the absolute pressure on the centerline of the torch vs axial distance. This plot vividly shows the magnitude of the pressure changes due to the expansion and compression waves intersecting the centerline flow exterior to the aircap. The pressure decreases from 200 kPa (2.0 atm) in the exit plane of the aircap to a minimum of 50 kPa (0.5 atm) at the maximum influence of the expansion waves. The first shock wave, that is, the

beginning of the first shock diamond, begins at about 17 mm and then compresses the flow to roughly 130 kPa. This pattern can be seen repeating itself such that four shock diamonds can be identified before the flow stabilizes at atmospheric pressure. As will be seen later, the flow on the centerline at the exit of the computational domain is slightly supersonic.

Contours of gas temperature over the entire computational domain are shown in Fig. 8. Three of the four shock diamonds noted in the previous graph of pressure are visible as regions of elevated temperature in this contour plot. In a previous section, a qualitative description was given of the structure of an under-expanded supersonic jet. That description, however, assumed uniform, Mach one flow at the exit of the aircap. As one would suspect from the previous internal flow description and these temperature contours, the HVOF jet structure will be much more complex. For example, Fig. 8 suggests that the shock diamonds would be irregular, particularly the first shock diamond because of the lower temperature argon flow. The luminosity of the center of the first shock diamond would be much less than off the centerline. This plot also shows the axial distance required for the low temperature argon carrier gas to be mixed with the surrounding high temperature stream. By an axial position of about 30 mm the low gas temperature along the centerline is essentially gone, that is, the peak temperature occurs on the centerline. After this point, the cooling of the HVOF jet by mixing with the ambient air becomes the dominant characteristic.

Figure 9 shows the temperature along the centerline of the torch vs axial distance. This plot exemplifies the complexity of the multiple stream mixing in the HVOF torch being analyzed. This shows that the centerline temperature remains at room temperature until 9 mm from the face of the nozzle. The rapid rise in temperature between 9 and 13 mm is due to mixing of the combustion gases with the cool argon/particle stream. Over this same distance, however, the flow surrounding this core flow is expanding supersonically, that is, the surrounding gas temperature is decreasing. This characteristic becomes dominant between 13 and 17 mm where the temperature decreases due to supersonic flow expansion. As mentioned earlier, the first shock diamond begins at 17 mm and this compression increases the gas temperature. Shock heating combines with the increase in temperature due to combustion gas mixing to cause a continued increase in temperature.The second expansion region begins at 21 mm and causes a drop in temperature, overpowering the increase in temperature due to mixing. After 30 mm, two more weak expansion and compression regions cause the temperature to oscillate but with decreasing amplitude. After 50 mm, the centerline temperature monotonically decreases due to mixing with the cool ambient air.

The u-component of velocity vs radius for axial locations of 10, 25, 50, and 75 mm is shown in Fig. 10. At the exit of the aircap, x = 10 mm, the velocity varies from 200 m/sec on the centerline, to 1550 m/sec in the center of the combusting stream. This factor of eight variation in velocity shows the importance of why these type HVOF torch designs must be analyzed using two-dimensional CFD techniques instead of one-dimensional flow analyses. One dimensional analyses assume fully mixed flow at each axial station and, therefore, they are not able to capture the required flow physics. Also seen at x =10 mm is the sharp decrease in velocity through the

turbulent boundary layer near the wall of the aircap (r = 3.62 mm). At x = 25 mm the ratio between the peak velocity and the centerline velocity has decreased to 1.8. The gas velocity on the centerline peaks at x = 20 mm at 1000 m/sec and the peak velocity in the combusting stream peaks at 1660 m/sec at about the same location. Near the end of the computational domain, x = 75 mm, the velocity deficit on the centerline has essentially disappeared. From this point on, the decay of the velocity profiles are similar to those from a hot jet with uniform velocity at the exit plane.

Figure 11 shows the contours of local Mach number for the torch. It is clearly seen from these contours of Mach number that an annulus of supersonic flow persists even through the compression waves associated with the shock diamonds. The peak Mach number in this annulus is roughly 1.9. In the center of the stream, however, the jet is subsonic until x = 13 mm at which point it attains Mach one. Continued mixing of the core flow and also the supersonic expansion waves result in a peak Mach number on the centerline of 1.6 at x = 17 mm. After this point, the normal shock wave near the centerline causes the Mach number to become subsonic and decrease to a value of 0.4 at 20 mm. The flow accelerates after the shock diamond and becomes supersonic again, and is processed by two more compressions and expansions. It is also noted in Fig. 11 that the flow near the centerline at the outflow boundary of the computational domain is supersonic, M = 1.1. The centerline Mach number decreases very slowly for x > 60 mm because as the local velocity decreases, the local speed of sound is also decreasing due to the cooling of the jet. This results in a nearly constant Mach number.

Particle Characteristics. Recall from the CFD formulation [3], eight computational particles were introduced in the argon stream. Each of these computational particles represents a large number of actual copper particles in the stream, all with a diameter of 30 μm. The mass, momentum, and energy equations of the gas are fully coupled to the mass, momentum and energy equations of the particle. The computational particles are distributed evenly across the argon stream at the same temperature and velocity of the argon. Figure 12 shows the trajectory of each of the eight computational copper particles. Note that the radial scale is greatly expanded, roughly a factor of 30, to show the small radial motion of the particle trajectories. Outside of the aircap, the simulation predicts all particles are within 0.7 mm of the centerline at x = 80 mm. Because of the complex interaction of particles with turbulent eddies in the gas, which is not in the present simulation, it is believed particles will be dispersed further from the centerline than the present simulation predicts.

Although the particles are introduced across the argon stream, up to 1.5 mm from the centerline, the 5^{o} radial component of velocity in the oxy-propylene stream moves all of these particles to within 0.7 mm of the centerline. An interesting feature of the trajectories is the apparent "bouncing" of two of the particles on the centerline, one near 38 mm and one near 52 mm. The CFD code computes any impact of a solid particle on a surface as a specular reflection. Although the centerline is not a surface, it is a line of mirror symmetry in axisymmetric flow. As a result, the computational interpretation of the "bouncing" of the particles is simultaneous impact of particles with their mirror image from the opposite side of the line of symmetry. Physically, the probability of this collision on the centerline is near zero. Reinterpreting the computational "bouncing," one

can conclude that the reflection is physically a particle traversing from the other side.

Figure 13 shows the temperature of each of the eight particles vs axial position. Also shown in the plot is the temperature of the gas on the centerline, as the particles are near the centerline. The particles show a range in temperatures, depending where they were introduced in the argon stream. Particles near the edge of the argon stream are exposed the highest gas temperatures because of the mixing layer with the combustion stream. It can be seen that the two particles near the edge of the argon stream are the only particles that attain the melting temperature of pure copper, 1358 K. These two computational particles that attain the melting temperature, however, have not absorbed sufficient heat to fully melt the particles. They are 20% and 8% melted, respectively, when they exit the computational domain. As the gas temperature at the edge of the computational domain has nearly dropped to the particle melt temperature, it can be concluded that none of the copper particles will fully melt.

Predicted particle velocities vs axial position, along with the velocity of the gas on the centerline, are shown in Fig. 14. At the exit of the aircap the velocity of the particles ranges from 20 m/sec to 60 m/sec, depending on their location when introduced into the argon stream. As was discussed earlier, the explanation for the low particle velocities at the aircap exit is the very low gas velocities near the centerline in the aircap (see Figs. 5 and 10). External to the aircap they increase in speed steadily, although their velocities are not as high as is commonly believed for HVOF spraying. As the particles exit the computational domain, they are predicted to be in the range of 220 to 240 m/sec.

An interesting feature to note from the particles velocities is their response to the expansion waves and shock waves in the jet. Small particles, for example, less than 0.1 μm, respond to rapid changes in velocity, but large particles tend to be unresponsive. From Fig. 14, the most rapid acceleration of the particles occurs in the region of increase in velocity along the centerline due to argon mixing with the combustion stream. Recall from Fig. 11 that Mach one on the centerline occurs at 13 mm. The beginning of the first shock diamond is at x = 17 mm (Fig. 7) and it is seen from Fig. 14 that there is some response of the particle to the shock wave. A change of slope of velocity, i. e., acceleration, occurs beginning at this point. The particles continue to accelerate through the shock diamond, but their rate of increase in velocity is decreased. This is because the particle velocity is still less than the subsonic gas velocity. After the first shock wave, the influence of the shock diamonds on the particle velocity is not noticeable because the strength of the shock waves steadily decreases as more occur.

Summary and Future Work

During the last few years, the thermal spray community has seen new experimental and computational approaches and viewpoints. Researchers from aerospace and defense applications have begun applying their efforts to the topic of thermal spraying. In addition, many of these researchers come from a background in gas dynamics, heat transfer and two-phase flow, thereby

adding a new perspective to the strongly interdisciplinary field of thermal spraying. This paper describes the general gas dynamic features of HVOF spraying and then gives a detailed discussion of the computational predictions of the present analysis. The gas velocity, temperature, pressure and Mach number distributions are presented for various locations inside and outside the torch. Also presented and discussed are the characteristics of the metal spray trajectories, particle velocity, and temperature.

Future work will include development of a finite rate chemical reaction model. Use of this type model will improve the prediction of the flow velocities and gas temperatures inside the aircap. Although the present instantaneous chemistry model yields the correct energy added to the flow field, its rapid release of energy near the nozzle over-predicts gas velocities. The detrimental effects of this over-prediction can be better judged by comparing it with a finite rate chemistry model. Also planned in future work is the measurement of pressures inside the aircap and gas and particle velocities exterior to the aircap. These measurements are critical to build confidence in the present mathematical and numerical modeling.

Acknowledgement

We would like to thank Fritz Owens and Anantha Krishnan of CFD Research Corp. for their technical assistance and consultations. We also thank Amalia Lopez of Sandia National Laboratories for her generous assistance.

References

1. Power, G. D., T. J. Barber, and L. M. Chiappetta, "Analysis of a High Velocity Oxygen-Fuel (HVOF) Thermal Torch," AIAA Paper No. 92-3598, AIAA/SAE/ASME/ASEE 28th Joint Propulsion Conf., Nashville, TN, July, 1993.
2. Smith, E. B., G. D. Power, T. J. Barber, and L. M. Chiappetta, "Application of Computational Fluid Dynamics to the HVOF Thermal Spray Gun," International Thermal Spray Conf., Orlando, FL, May, 1992, 805-810.
3. Oberkampf, W. L. and M. Talpallikar, "Analysis of a High Velocity Oxygen-Fuel (HVOF) Thermal Torch, Part 1: Numerical Formulation," Proceedings of the 7th National Thermal Spray Conf., Boston, MA, June, 1994.
4. Hackett, C. M., G. S. Settles, and J. D. Miller, "On the Gas Dynamics of HVOF Thermal Sprays," Proceedings of the 6th National Thermal Spray Conf., Anaheim, CA, June, 1993, 167-172.

DISCLAIMER

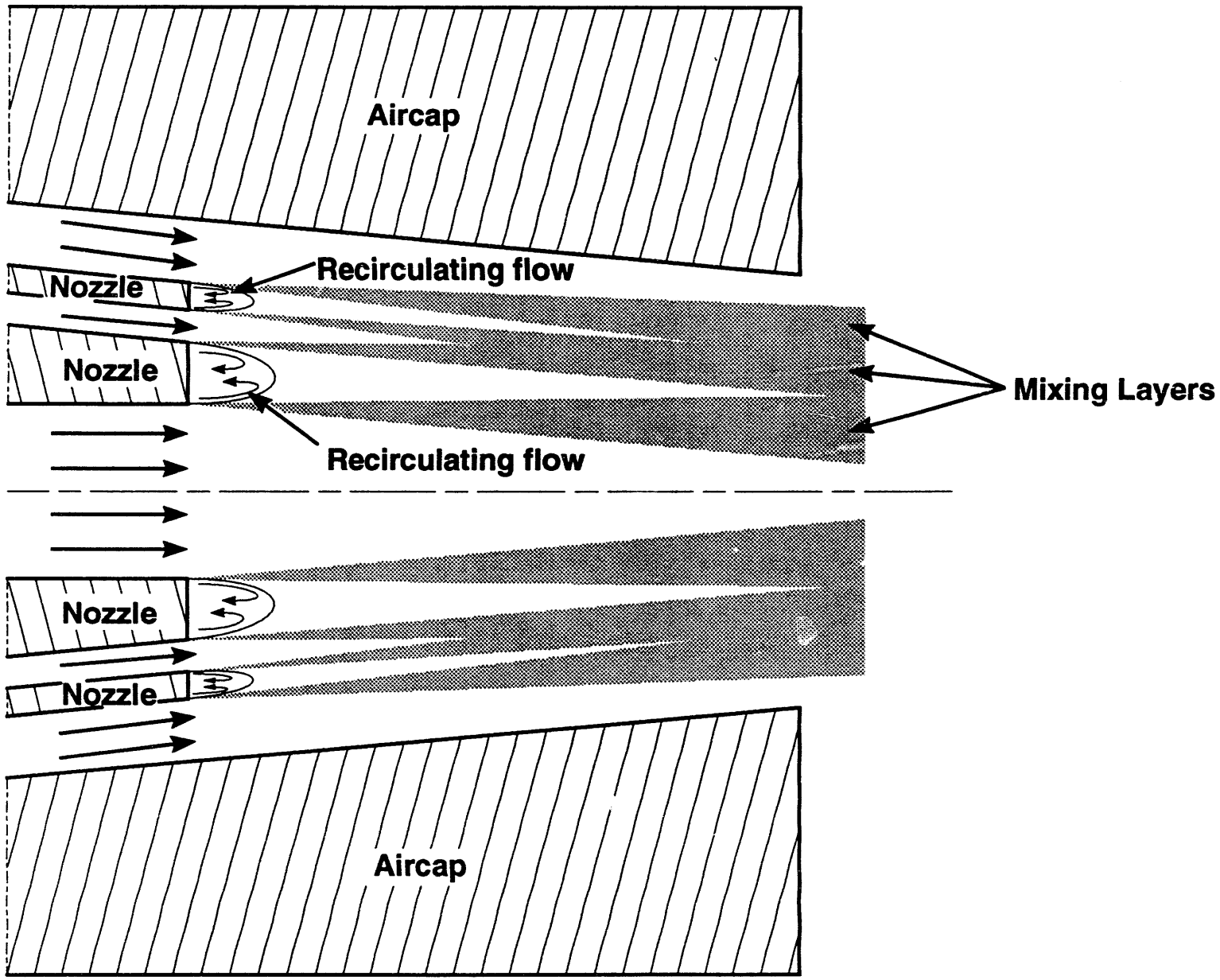

Figure 1: Recirculating Flows and Mixing Layers Inside Aircap

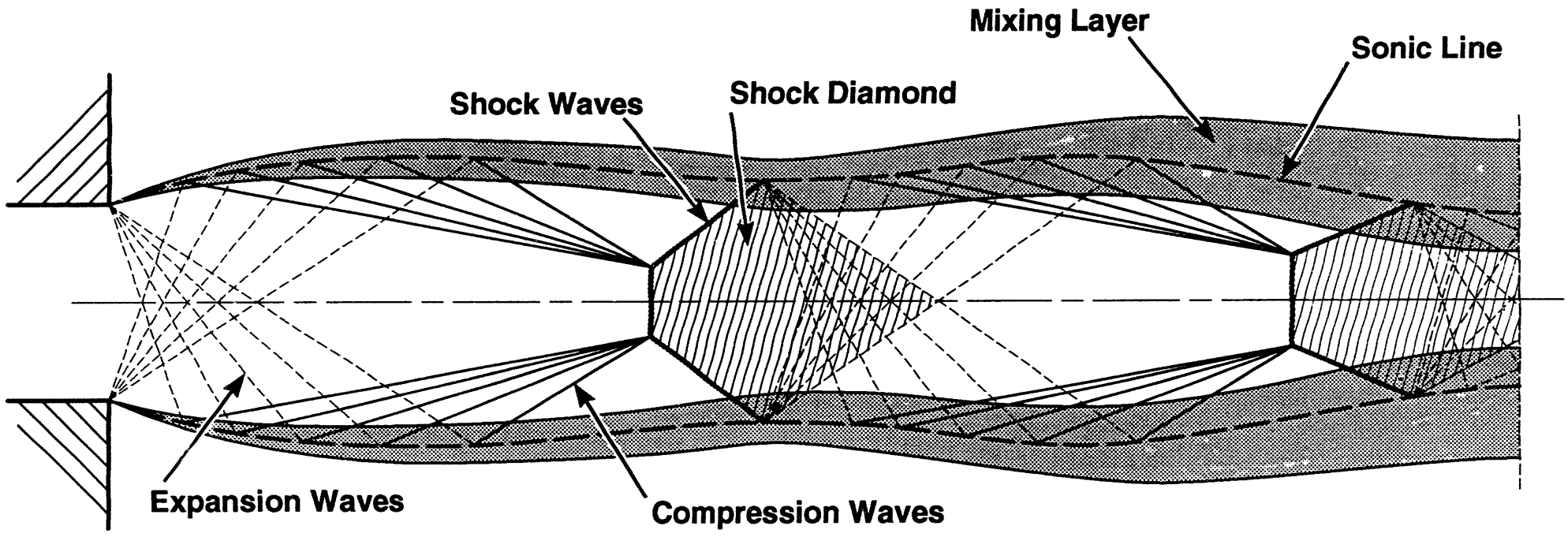

Figure 2: Mixing Layer and Wave Structure in Supersonic Underexpanded Jet

(2D) || Print || 4 Jan 1994 || fin.plt ||

Figure 3: Temperature Contours Inside Aircap

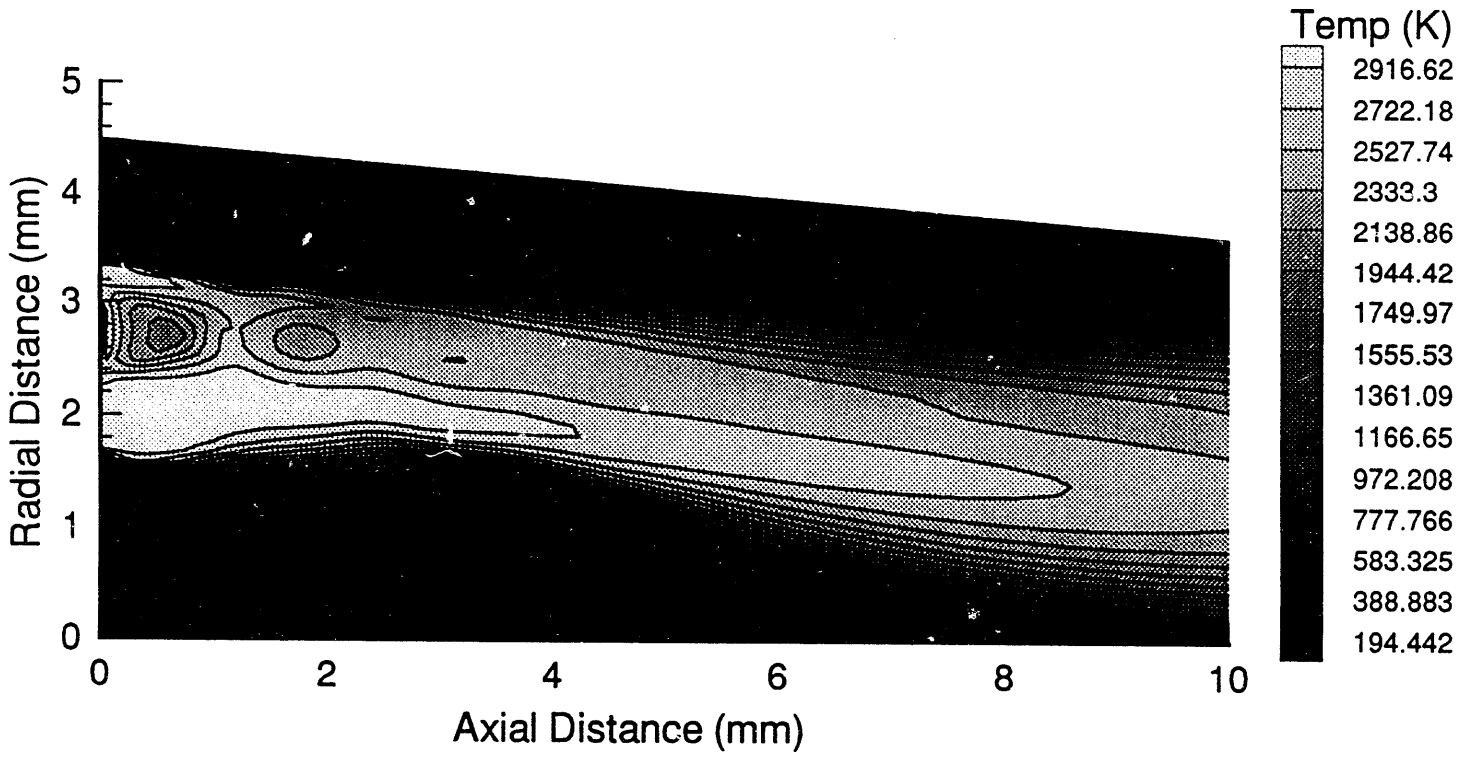

(2D) || Print || 4 Jan 1994 || fin.plt ||

Figure 4: Mach Number Contours Inside Aircap

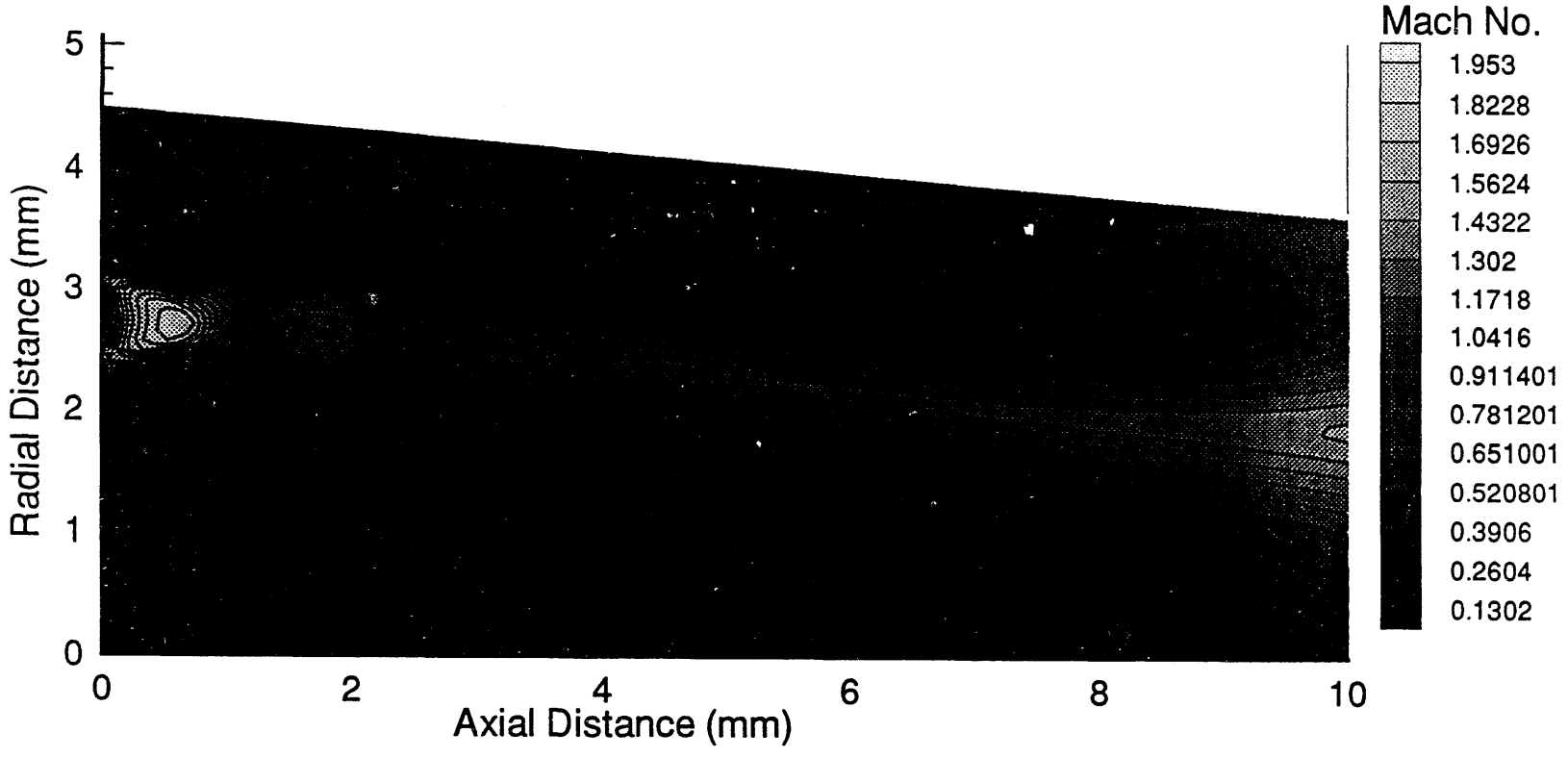

Figure 5: Axial Velocity Profiles Inside Aircap

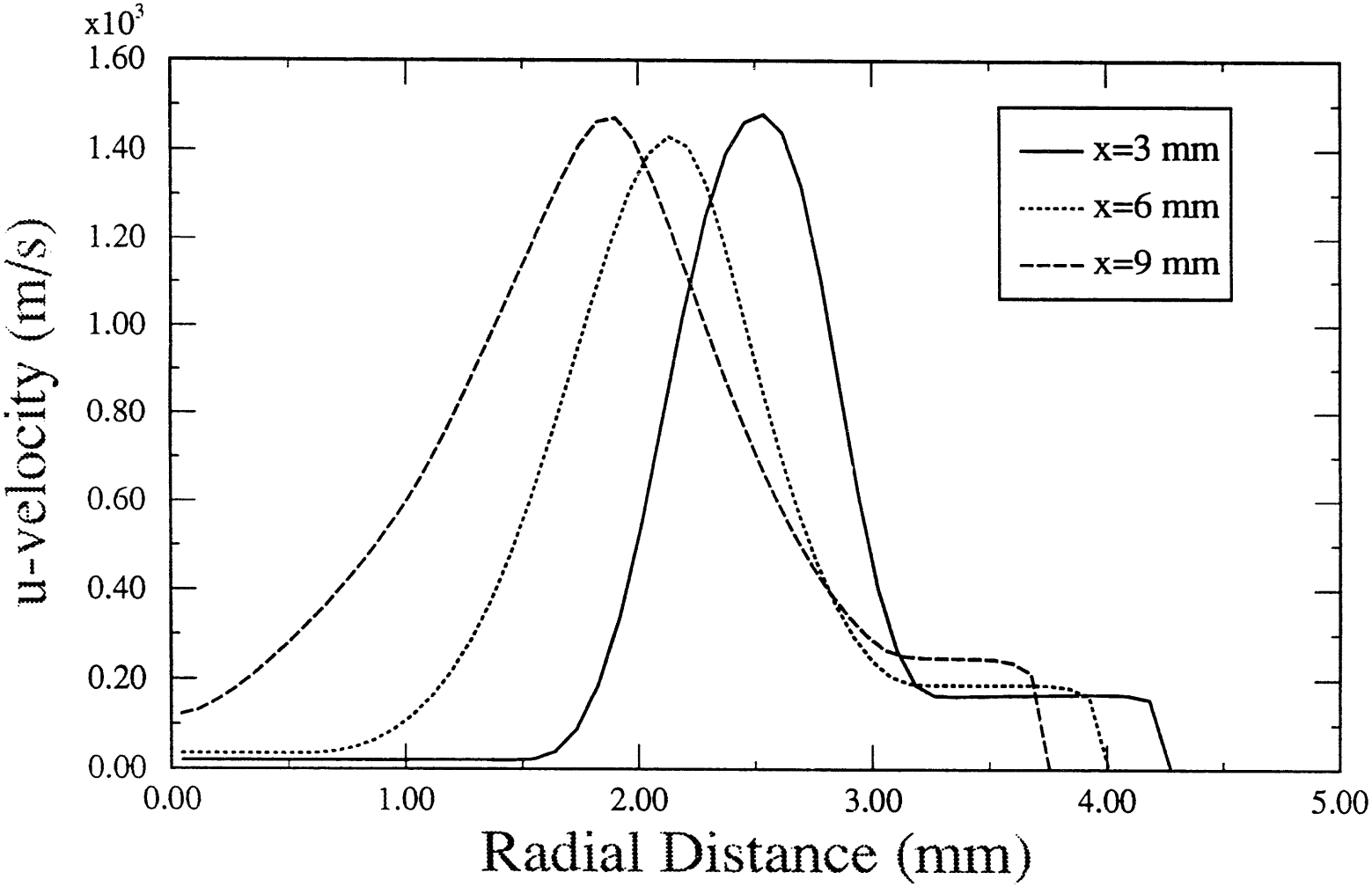

TempleGraph 2.6, Origin: wloberk@sass857 - Tue Jan 4 16:42:29 1994 (data file was u.r.9.dat)

(2D) || Print || 5 Jan 1994 || fin.plt ||

Figure 6: Static Pressure Contours Inside Aircap

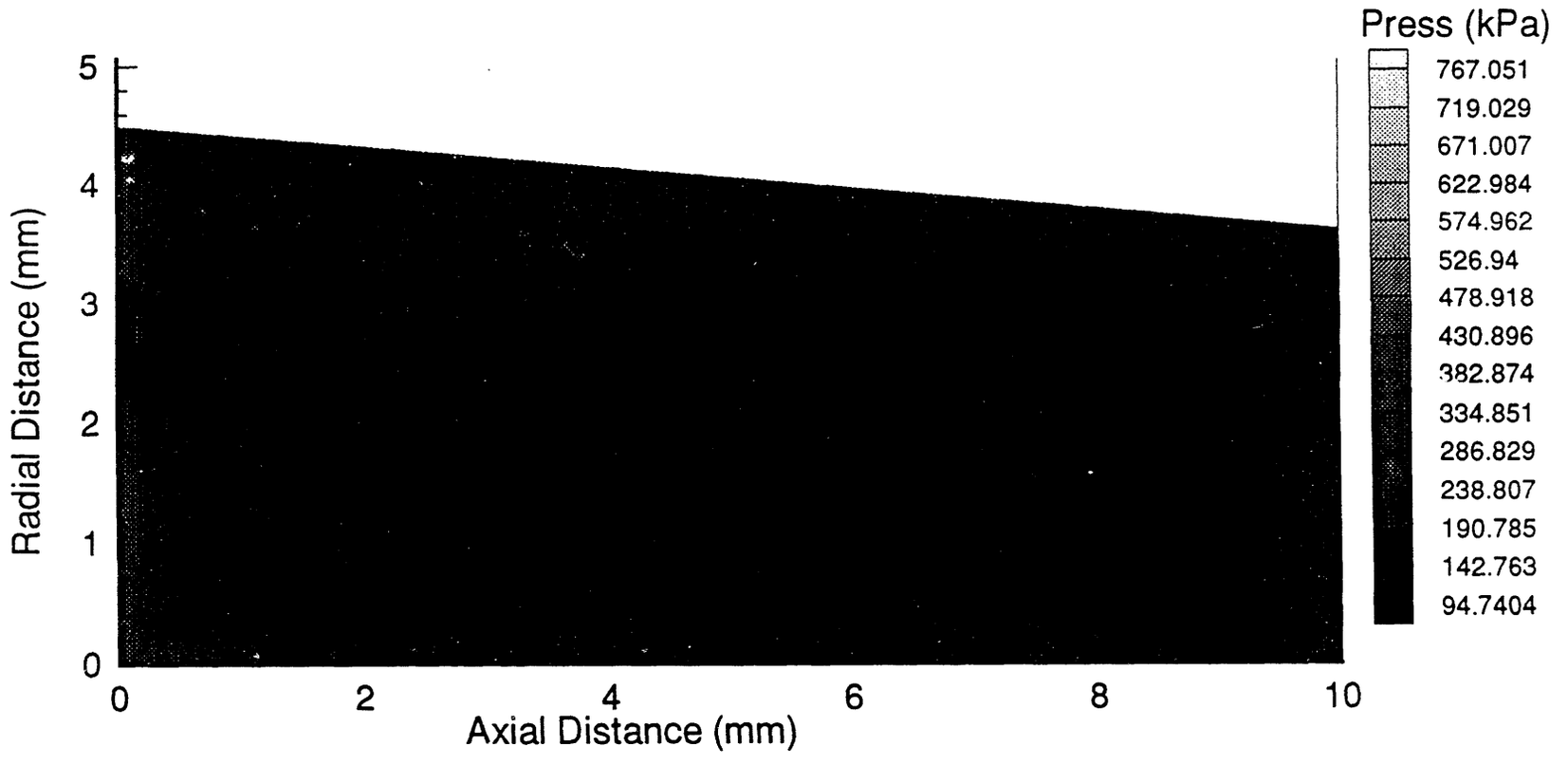

Figure 7: Static Pressure vs Axial Distance Along Centerline

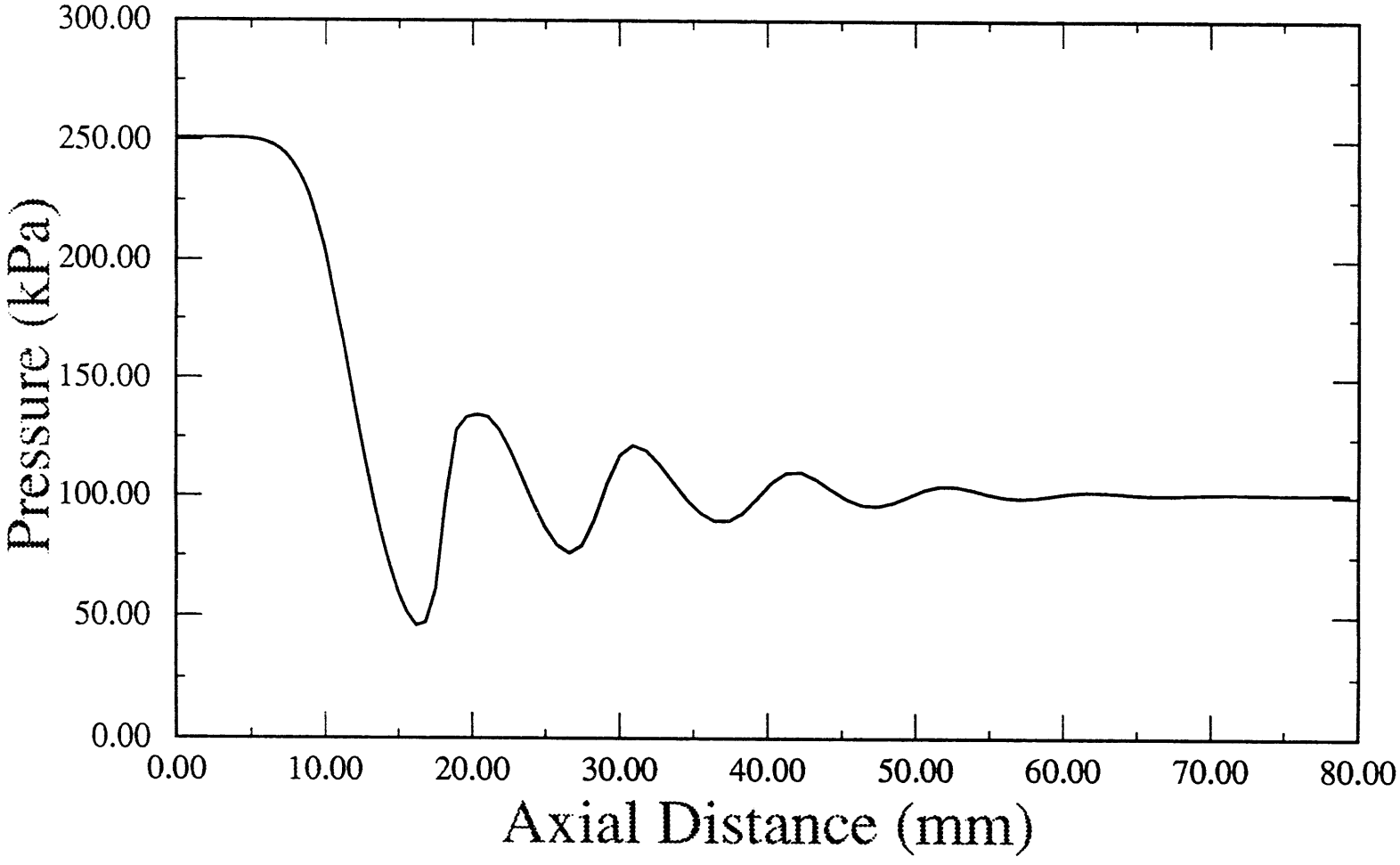

TempleGraph 2.6. Origin: wloberk@sass857 - Wed Jan 5 10:01:50 1994 (data file was /u4/wloberk/CFDRC/sandia_case1/instant.chem.spray/pres.x.mif.data)

(2D) || Print || 4 Jan 1994 || fin.plt ||

Figure 8: Temperature Contours Over Computational Domain

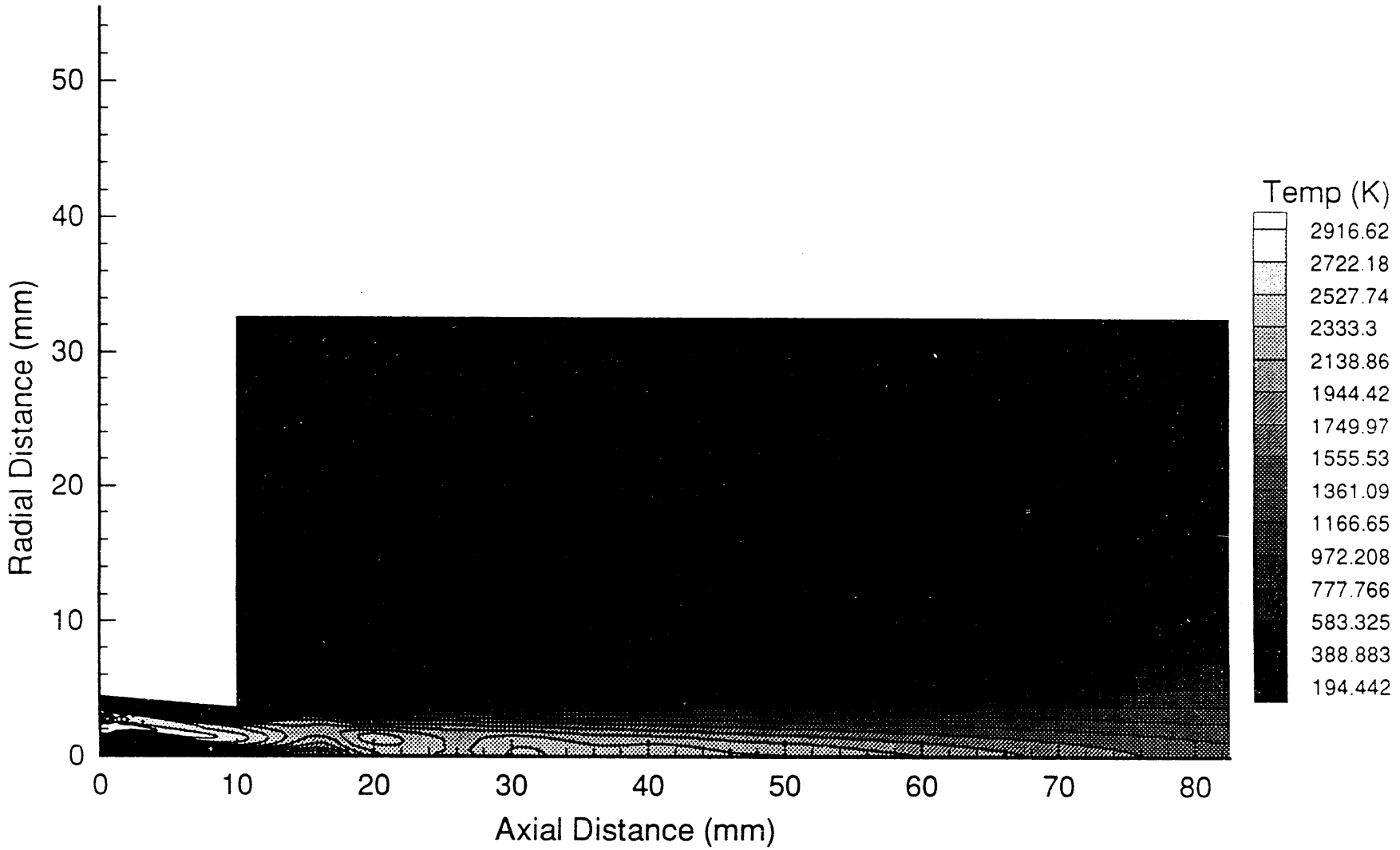

Figure 9: Temperature vs Axial Distance Along Centerline

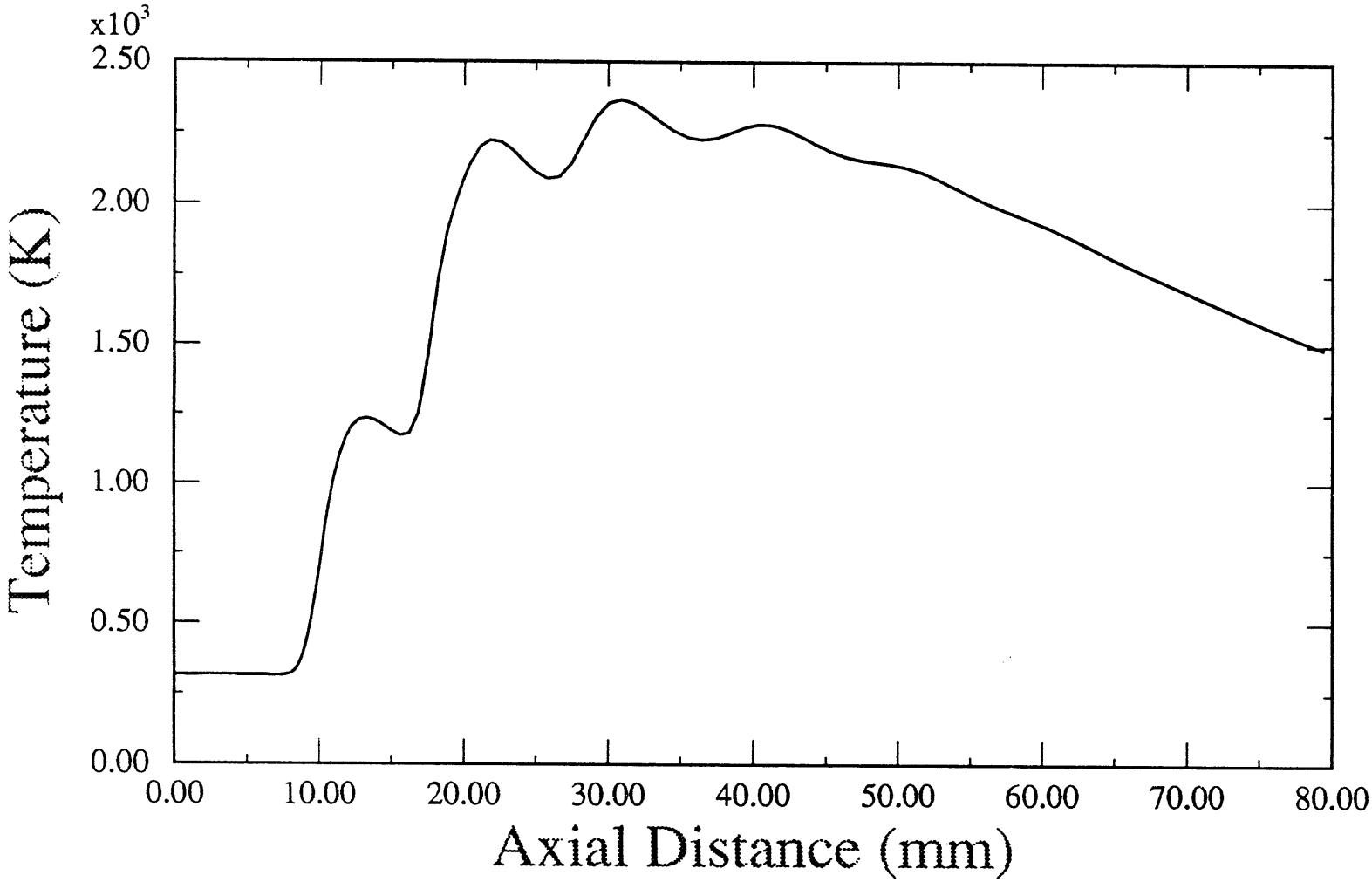

TempleGraph 2.6, Origin: wloberk@sass857 - Tue Jan 4 16:33:20 1994 (data file was temp.x.dat)

Figure 10: Axial Velocity Profiles Outside Aircap

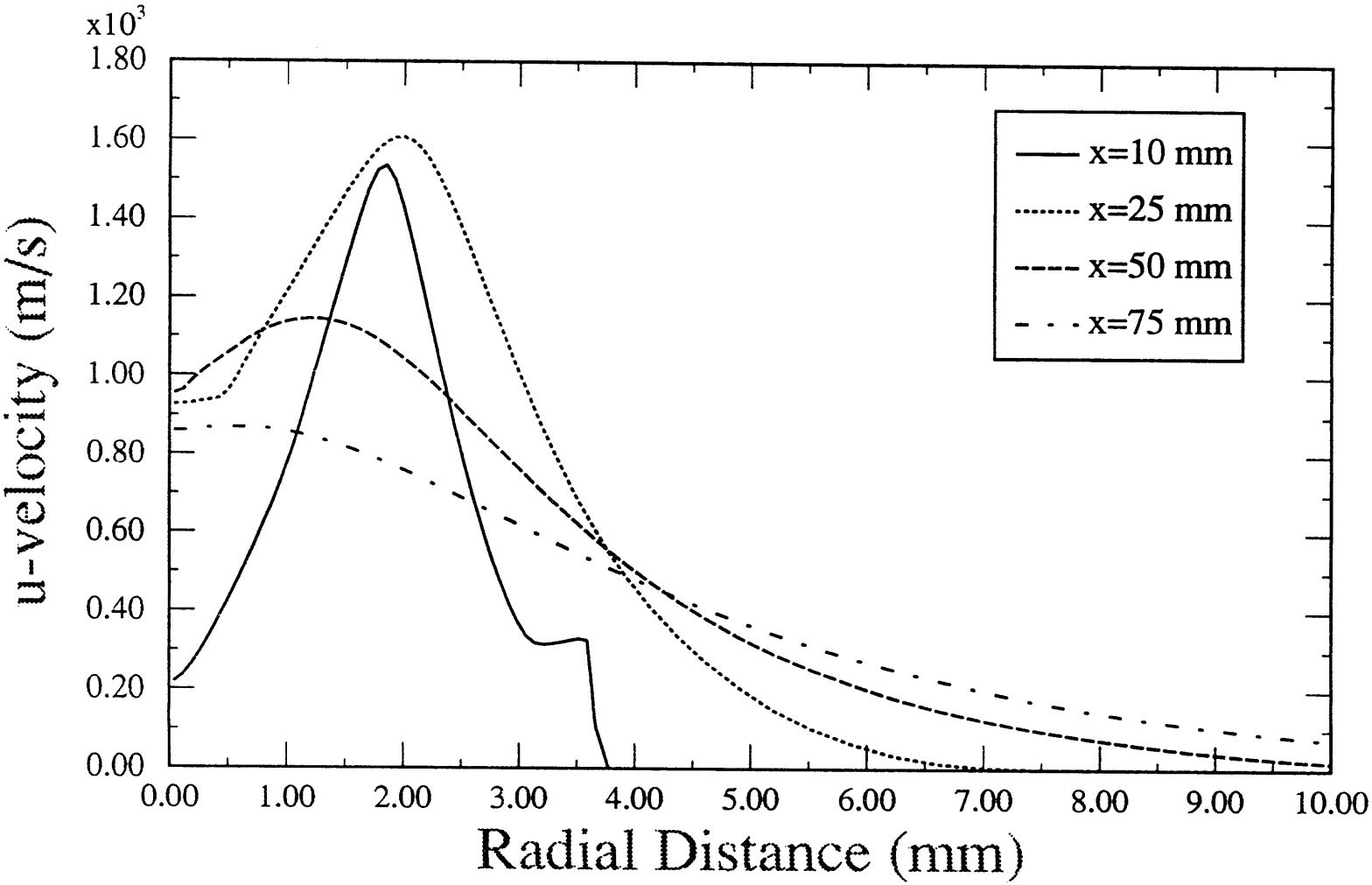

TempleGraph 2.6, Origin: wloberk@sass857 - Tue Jan 4 16:49:52 1994 (data file was u.r.75.dat)

(2D) || Print || 4 Jan 1994 || fin.plt ||

Figure 11: Mach Number Contours Over Computational Domain

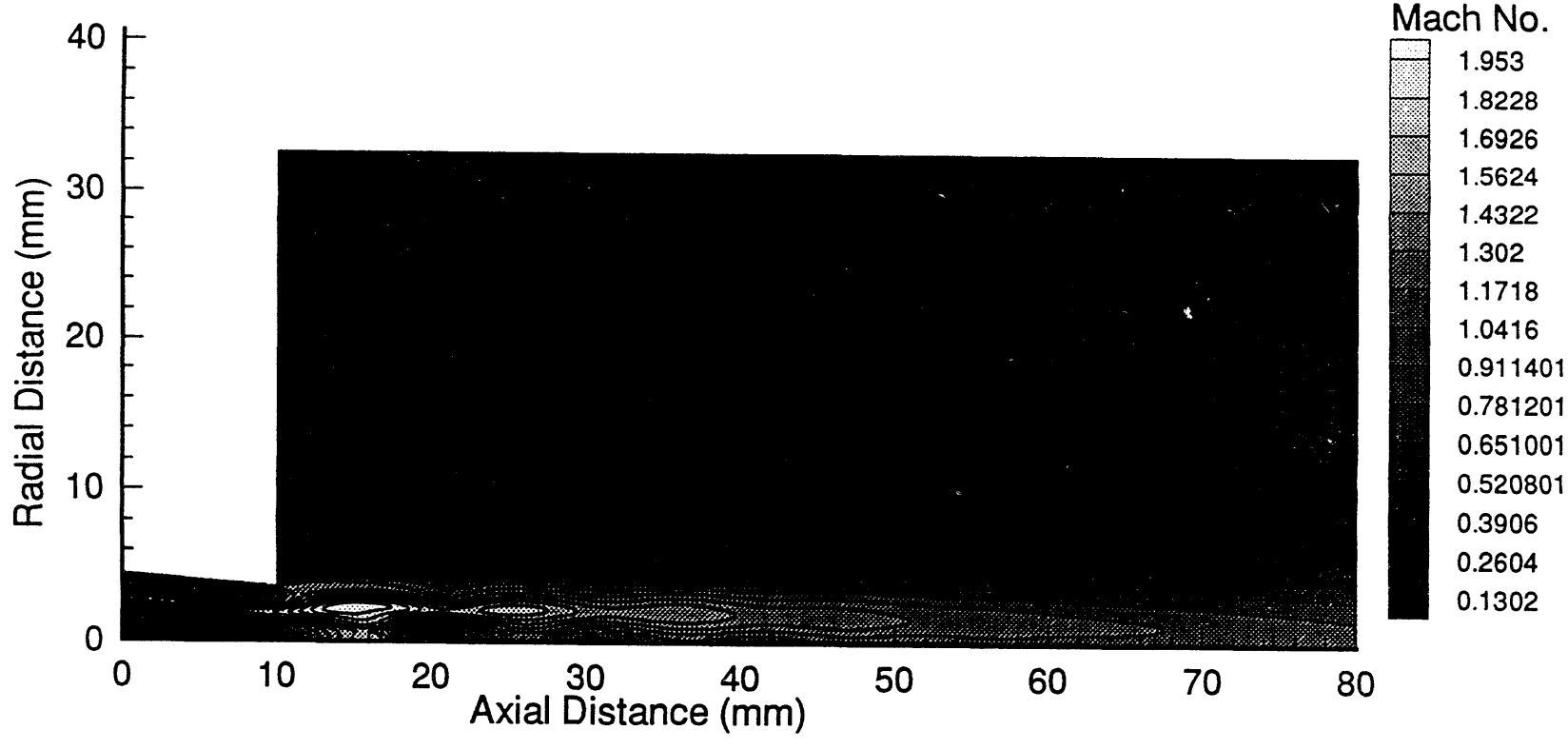

Figure 12: Particle Trajectories

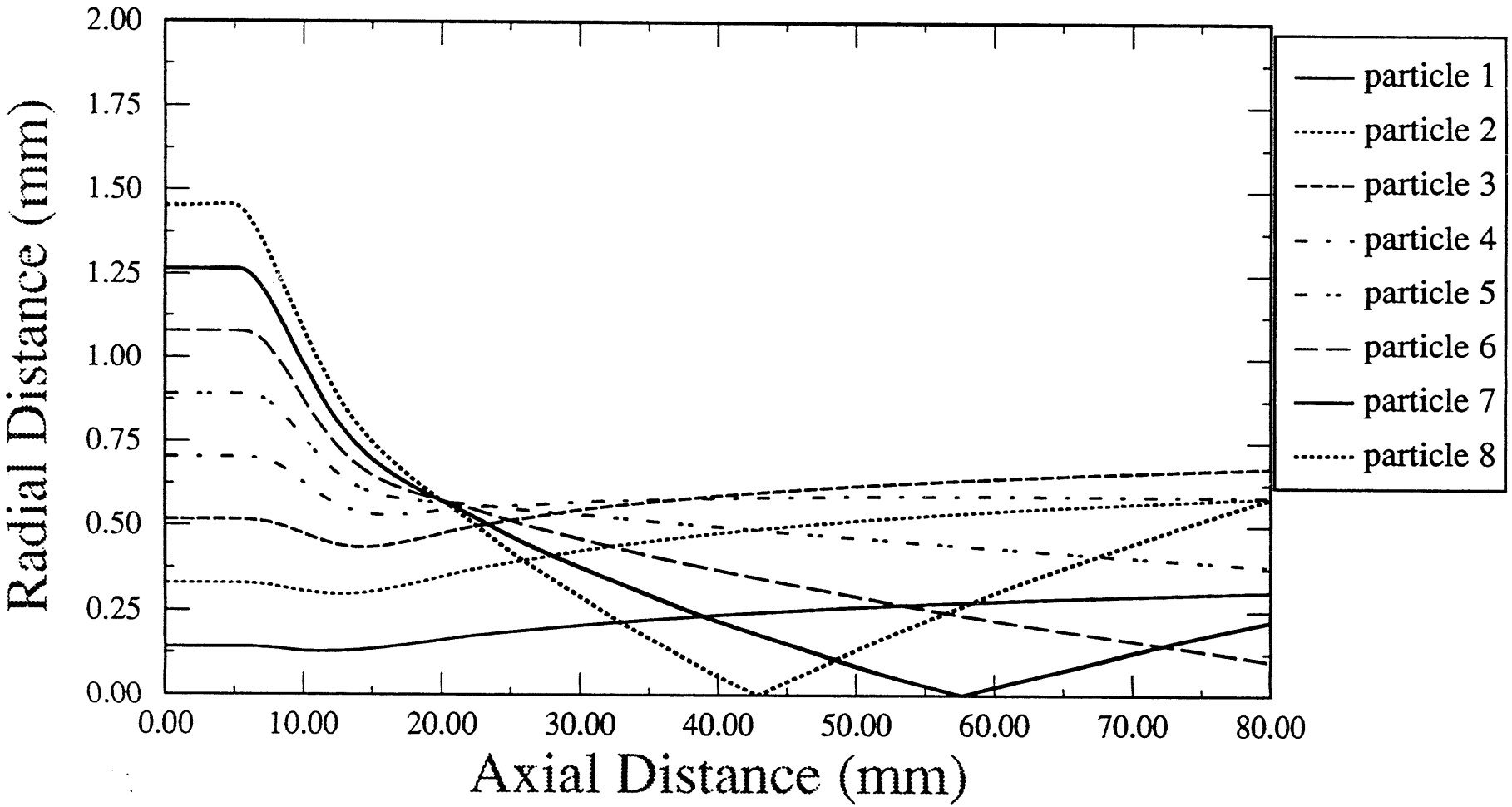

TempleGraph 2.6, Origin: wloberk@sass857 - Wed Jan 5 09:57:08 1994 (data file was pd8.dat)

Figure 13: Particle Temperatures vs Axial Distance

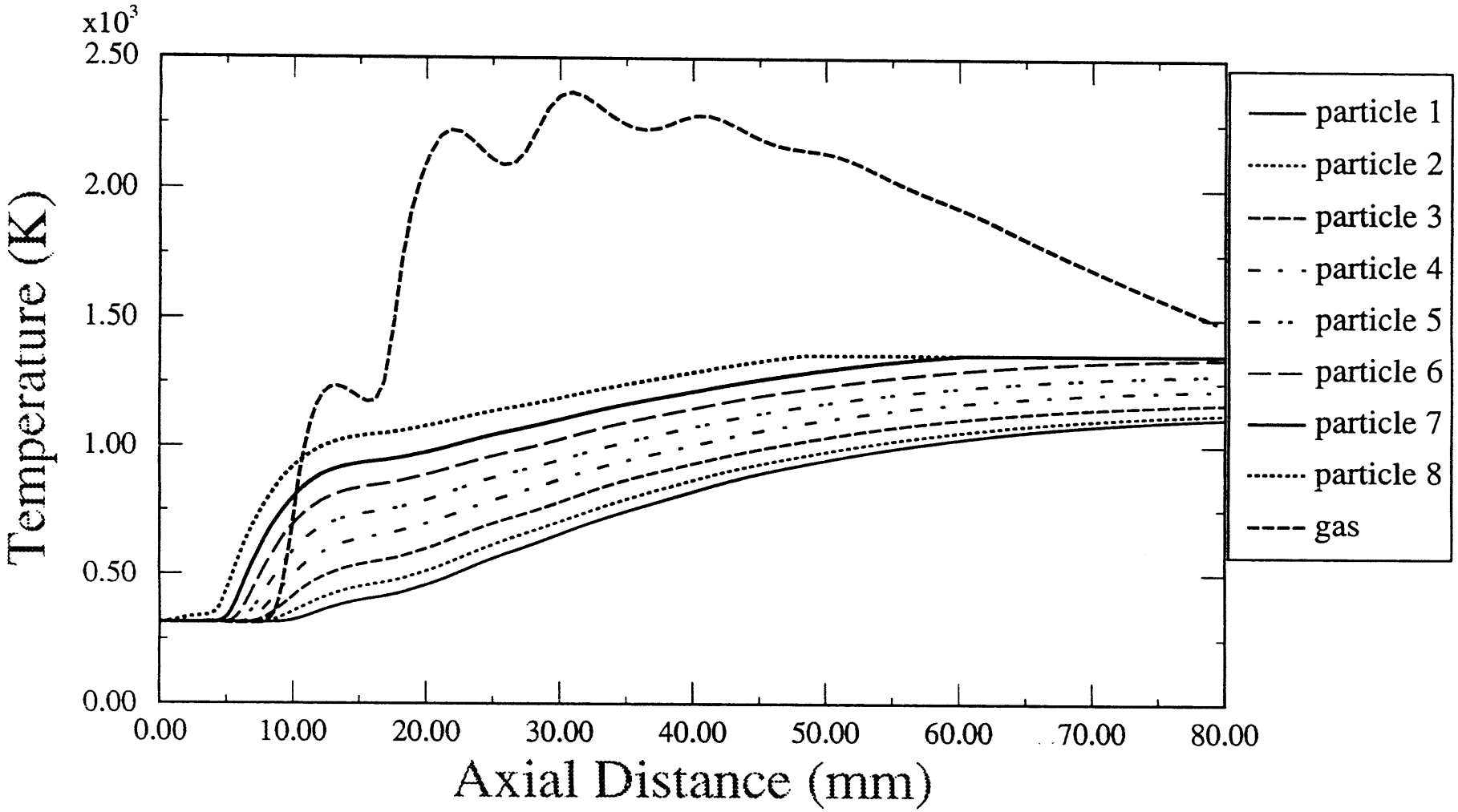

TempleGraph 2.6, Origin: wloberk@sass857 - Tue Jan 4 17:02:37 1994 (data file was temp.x.dat)

Figure 14: Particle Velocities vs Axial Distance

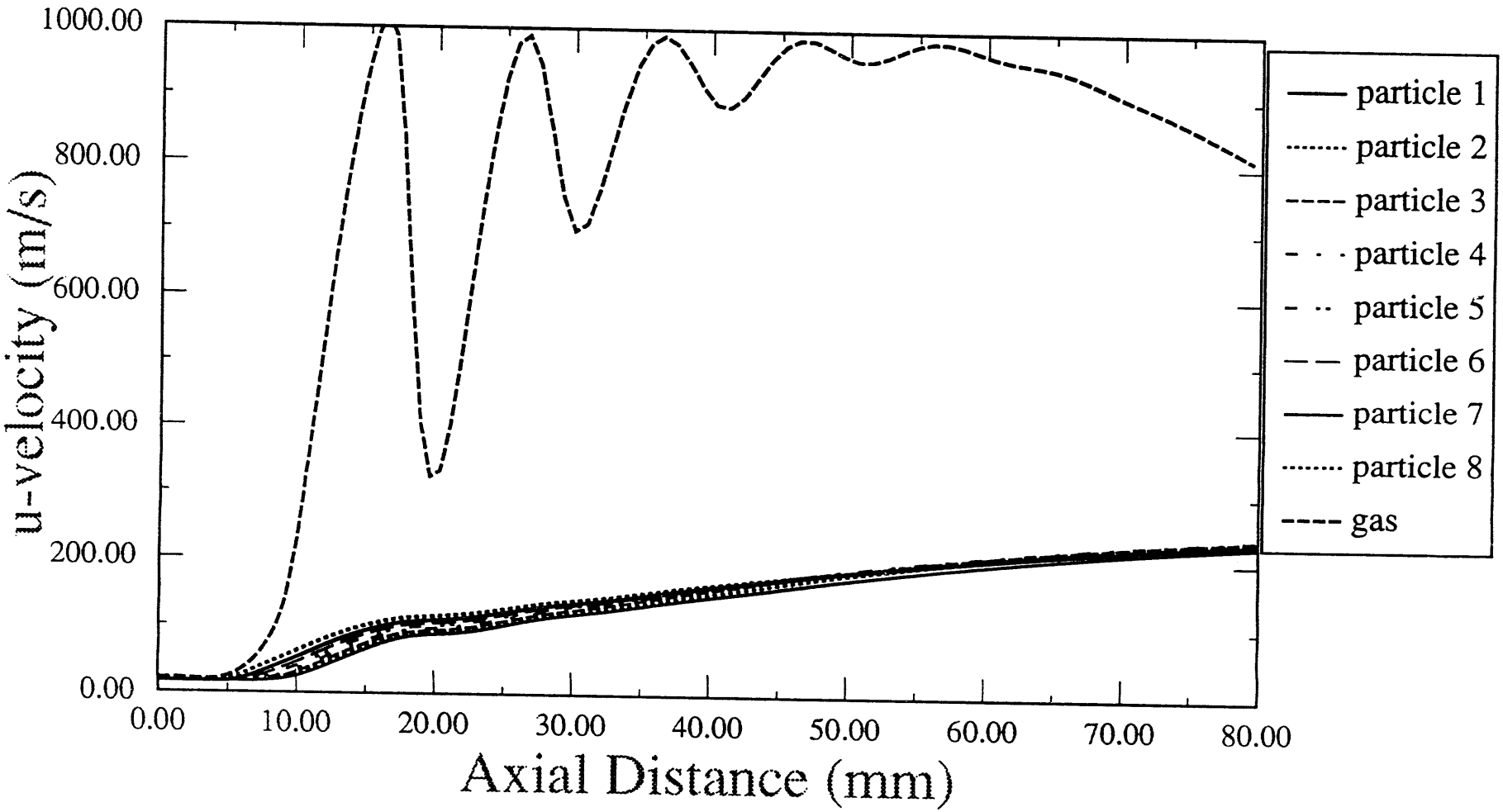

TempleGraph 2.6, Origin: wloberk@sass857 - Tue Jan 4 17:09:15 1994 (data file was u.x.dat)

DATE
FILMED
5/9/94
END